
Article:
Zhang, Y., Zhang, K., Hu, Z. et al. (2023) A modified highly stressed volume (HSV) method to predict fatigue life considering the critical crack size. International Journal of Fatigue, 172. 107644. ISSN: 0142-1123

https://doi.org/10.1016/j.ijfatigue.2023.107644

A modified highly stressed volume (HSV) method to predict fatigue life considering the critical crack size

Yating Zhang[1,2], Kun Zhang [1,2,*], Zheng Hu [3], Tianyu Chen[1], Luca Susmel[4], Bingchen Wei [1,2,*]

[1]Key Laboratory of Microgravity (National Microgravity Laboratory), Institute of Mechanics, Chinese Academy of Sciences, Beijing 100190, China

[2]School of Engineering Science, University of Chinese Academy of Sciences, Beijing 100049, China

[3]Science and Technology on Vehicle Transmission Laboratory, China North Vehicle Research Institute, Beijing, 100072, China

[4] Department of Civil and Structural Engineering, The University of Sheffield, Sheffield, S1 3JD, UK

Email: zhangkun@imech.ac.cn; weibc@imech.ac.cn

Abstract

Fatigue life prediction is important in engineering design to ensure structural reliability. However, it is difficult to achieve an accurate fatigue life prediction from a smooth specimen to a notched specimen with the traditional Highly Stressed Volume (HSV) method, as it is based on just one empirical evaluation of the HSV. A modified HSV method is proposed in this study, which is combined with the concept of critical distance, and the critical crack size of smooth specimens is obtained by observing the fracture surface. The predicted *P-S-N* curves of single-notched specimens and multi-notched specimens show a good agreement with experimental data compared with the traditional HSV method and the Theory of Critical Distance method.

Keywords: Fatigue life prediction; The crack initiation size; Critical distance; Highly stressed volume;

Fracture surface

Nomenclature

A	Material constants	S_S	The highly stressed surface area of a smooth specimen
B	Material constants	S_N	The highly stressed surface area of a notched specimen
E	Young's modulus	V_C	Highly stressed volume of specimen C
k	shape parameter of Weibull distribution	V_N	Highly stressed volume of notched specimen
T	Scatter index	Ps	The values of the probability of survival
$F_{N_C}(x)$	Weibull distribution function of specimen C	V_S	Highly stressed volume of a smooth specimen
$F_{N_S}(x)$	Weibull distribution function of a smooth specimen	β	Scale parameter of the Weibull distribution
$F_{N_P}(x)$	Weibull distribution function of a predicted specimen	ε_f	Fracture strain
K_t	Stress concentration factor	$\Delta\sigma_0$	The range of plain fatigue limit
ΔK_{th}	The range of threshold value of the stress intensity factor	σ_S	Yield strength
L_{CD}	The critical distance of notched specimens	σ_t	Ultimate tensile strength
L_{FCI}	The average depth of the FCI region	σ_{appl}	Applied stress
N_C	The fatigue life of specimen C	σ_{eff}	Effective stress
N_S	The fatigue life of smooth specimen	σ_{mp}	Max principal stress

1. Introduction

Fatigue life prediction is one of the most important functional concerns in engineering design for reliability and durability during the development of a product, and for predicting the structural durability of a component. Many methods have been proposed to predict the fatigue lifetime of engineering components [1-6], such as the Theory of Critical Distance (TCD), Strain Energy Density (SED) method and Highly Stressed Volume (HSV) method. Among them, the HSV method is widely used due to its simplicity of formulation and low computational cost [7-10]. An empirical parameter n% is proposed to characterize the HSV of notched specimens, which assumes that fatigue initiation on components experiencing a stress gradient occurs essentially in the HSV. However, the empirical parameter does not have the same value in the literature related to the materials, load types and notch size, which will lead to the formation of non-uniform HSV and large errors in the final prediction results. For example, the concept of 95% HSV was first introduced for wrought material by Kuguel [11] to establish the relationship between specimen shape and stress distribution. In other studies [12, 13] it was used to evaluate the fatigue properties of ductile materials, but was not verified to be suitable for other materials. Later, the V90 criterion, *i.e*., 90% HSV, which was proposed by Sonsino [8], has been widely used for prediction in metallic components, considering that the crack initiation occurs in a region under the surface. However, for short-fiber reinforced specimens [14] and welded components [9], V80, *i.e*., 80% HSV, has proven to be more suitable, as it can capture more material to compensate for possible local inhomogeneities.

In addition, some researchers have sought to predict the fatigue life of notched specimens directly from smooth specimens using the HSV method, as the known *S*-*N* curves of smooth specimens allow faster assessment of the component fatigue life. However, since this empirical parametric model

overestimates the HSV of smooth specimens, a un-safe prediction band is generally obtained [10, 15]. Due to the disadvantages of the volume method, a highly stressed surface area ignored highly stress layer thickness is also developed by using the 90% empirical parameter to account for the statistical size effect [16]. Also, since the fatigue crack initiation life includes a region not restricted to the surface, a conservative fatigue life assessment is obtained [16, 17]. Generally, the crack initiation life occupies the majority of the total fatigue life of the components and it includes the early cyclic deformation, microcrack nucleation, and short crack extension [18-21]. Therefore, a definition of critical crack size considering the fatigue initiation regions of smooth and notched specimens is expected.

For notched components, fatigue cracks initiate from the notch root where the stress concentration occurs, and the initiation of fatigue cracks is mainly driven by the local cyclic stress and strain at the notch root [22, 23]. A characteristic material length was proposed by Neuber [24] to calculate the effective stress taking into account the effect of stress concentration. It was assumed that the initiation of fatigue cracks is determined by the average stress over a short distance, rather than the maximum principal stress. Base on this assumption, the critical distance proposed by Taylor [25] has been widely used to determine the fatigue initiation region, which considers the short cracks for stress concentrations of notched components. For smooth specimens, the fatigue crack initiation life is mainly determined by the formation of the persistent slip bands [20, 26, 27] and the stage of short crack propagation is smaller than that of notched specimens [28]. Thus, the critical distance is not suitable to replace the critical crack size in smooth specimens, and the definition of the critical crack size for smooth specimens is different from that for notched specimens. It is worth noting that the critical crack size of smooth specimens could be determined by investigating the fatigue fracture surface. The fatigue crack initiation region of smooth specimens shows a rougher fracture surface morphology compared to the crack propagation region [29].

Moreover, a number of studies have shown that the specimens of different materials, shape, and size exhibited different fracture characteristics [26, 30, 31]. Therefore, a question could be raised as to whether it is possible to build a bridge of the fatigue life between smooth and notched specimens by using the critical crack sizes.

The aim of this study is to establish a modified HSV method in which the critical crack size is used to describe the HSV of a smooth specimen by observing the fracture surface. The model is verified using both single-notched and multi-notched specimens, and the predicted *P-S-N* curves of single-notched specimens and multi-notched specimens show a good agreement with the experimental data compared with traditional HSV method and TCD method. The article is organized as follows: Section 2 describes the proposed modified HSV model. Section 3 validates the model using experimental data of single-notched and multiple-notched specimens. Also, the accuracy of the proposed model is compared with the HSV and TCD methods. Conclusions are given in Section 4.

2. Methods

2.1 Probability distribution model of the HSV method

Considering the statistical and geometrical size effects, a probabilistic HSV model based on the Weibull distribution is developed and used. The Weibull model has been extensively used to predict fatigue strength and life distribution [16, 27, 32]. In addition, it has been reported [33-35] that the Weibull model reflects the influences of the statistical and geometrical size effects. Based on the assumption that notched specimens and smooth specimens are composed of a number of small specimens denoted as specimen C, the Weibull distribution model for notched specimens can be formulated as:

$$F_{N_N}(x)=1-\left(\frac{x}{\beta(\frac{V_N}{V_C})^{-1/k}}\right)^k, \quad \cdots\cdots\cdots\cdots\cdots\cdots\cdots\cdots\cdots\cdots\cdots\cdots(1)$$

where β is a scale parameter. Under the same survival probability, it can be obtained that $1-F_{N_N}(x)=1-F_{N_C}(x)=1-F_{N_S}(x)$.

$$1-e^{-\left(\frac{N_N}{\beta n_N^{-1/k}}\right)^k}=1-e^{-\left(\frac{N_C}{\beta n_C^{-1/k}}\right)^k}=1-e^{-\left(\frac{N_S}{\beta n_S^{-1/k}}\right)^k}, \quad \cdots\cdots\cdots\cdots\cdots\cdots\cdots\cdots\cdots\cdots(2)$$

where $n_N=V_N/V_C$, $n_N=V_C/V_C=1$, $n_S=V_S/V_C$.

Then, the fatigue life prediction model under the same stress level can be described by equation (3) (Eq. (3)), which is obtained by combining Eqs. (1) and (2):

$$\frac{N_N}{N_S}=(\frac{V_N}{V_S})^{\mu}, \quad \cdots\cdots\cdots\cdots\cdots\cdots\cdots\cdots\cdots\cdots\cdots\cdots\cdots\cdots\cdots\cdots\cdots\cdots\cdots\cdots\cdots\cdots(3)$$

where N_N and N_S are the fatigue lives of notched and smooth specimens; V_N and V_S are the HSV of notched and smooth specimens; $\mu=-1/k$, k is the shape parameter which can be obtained by the Weibull distribution.

In the traditional HSV method, V_N and V_S in the Eq. (3) are usually derived by an empirical n% (described in detail in the Introduction). However, as indicated in the introduction the results predicted by the traditional HSV method could result in non-conservative estimates due to an overestimated HSV of smooth specimens. Therefore, the traditional HSV method needs to be modified.

To calculate the V_N and V_S in Eq. (3), the highly stressed surface area is used, which is defined as an area that does not exceed 90% of the maximum principal stress taking the statistical size effect into account [16]. In addition, the critical crack size, *i.e.*, high stress layer thickness of notched and smooth

specimens, considering the fatigue initiation mechanisms also need to be identified, which are referred to as the critical crack size and the details are given in the subsequent sections.

2.2 Determination of the critical crack size

Due to the different crack initiation mechanisms for notched and smooth specimens, different critical crack sizes are required to determine V_N and V_S in Eq. (3). For the V_N of the notched specimens, the critical distance based on Neuber's theory [24] is used to determine the critical crack size, since the fatigue initiation of notched specimens is controlled by the region under the surface. The critical distance (Fig. 1) depends on the material characteristics related to the transition point from short crack growth to long crack growth [36, 37], and it can be calculated by:

$$L_{CD} = \frac{1}{\pi}\left(\frac{\Delta K_{th}}{\Delta \sigma_0}\right)^2, \quad \cdots\cdots(4)$$

where ΔK_{th} is the range of the threshold value of the stress intensity factor calculated as $\Delta K_{th} = K_{th,max} - K_{th,min}$, and $\Delta \sigma_0$ is the range of plain fatigue limit calculated as $\Delta \sigma_0 = \sigma_{0,max} - \sigma_{0,min}$.

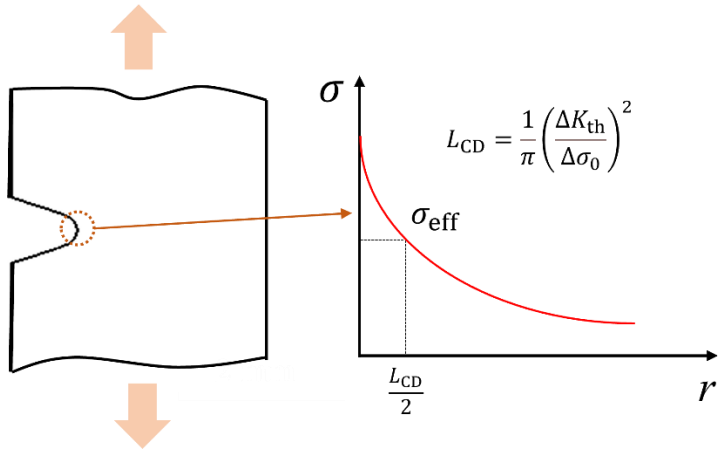

Fig. 1. Schematic plot of the stress as a function of distance from the notch root.

Therefore, V_N can be formulated as follows:

$$V_{\mathrm{N}} = S_{\mathrm{N}} \cdot L_{\mathrm{CD}}, \quad \cdots\cdots(5)$$

where S_{N} is the highly stressed surface area for the notched specimen.

For V_{S} of smooth specimens, the fracture surface is used to determine the critical crack size. In general, the fracture surface can be divided to the three regions shown in Fig. 2 (a), namely the fatigue crack initiation (FCI), propagation, and final rupture regions. The dislocations play a major role in the fatigue initiation region, and the persistent slip band can be observed due to a large number of loading cycles dislocation pile-up [29]. The extrusions or intrusions of the slip plane (Fig. 2 (b)) under forward and reverse loadings creates a rough fracture surface morphology in the crack initiation region [26, 27]. Moreover, some researchers have also sought to use a quantitative measurement of the fracture surface to calculate the fatigue damage accumulation [29, 31, 38]. Therefore, in this study, the critical crack size could be recognized by the fatigue fracture surfaces shown in Fig. 2, which can give an insight into the physical process by evaluating fracture surface roughness [26, 30, 31, 38], and it can be formulated as follows:

$$L_{\mathrm{FCI}} = \frac{L_1 + L_2}{2}, \quad \cdots\cdots(6)$$

where L_1 and L_2 are the depth of the FCI region along the edges, L_{FCI} is the average depth of the FCI region. Thus, V_{N} can be formulated as Eq. (7):

$$V_{\mathrm{S}} = S_{\mathrm{S}} \cdot L_{\mathrm{FCI}}, \quad \cdots\cdots(7)$$

where S_{S} is the highly stressed surface area for the smooth specimen.

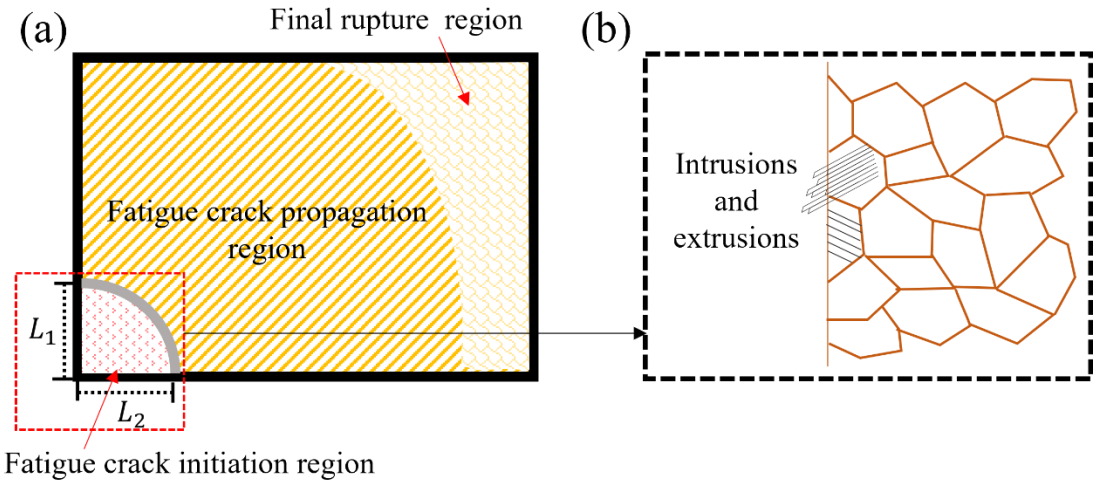

Fig. 2. Schematic representation of (a) fracture surface and (b) crack formation in the crack initiation region.

In addition, N_N is calculated under the same maximum principal stress used for the smooth specimen in the traditional HSV method. However, according to the notch effect, the fatigue strength of notched specimens is not controlled by the maximum principal stress, but by an effective stress averaged within the critical distance [24, 39]. The Point Method (PM) assumes that the effective stress σ_{eff} is the maximum principal stress σ_{mp} at half of the critical distance L_{CD} from the notch root, as shown in Fig. 1, which is expressed as Eq. (8):

$$\sigma_{eff} = \sigma_{mp}(r = \frac{L_{CD}}{2}), \quad \cdots\cdots(8)$$

Then, under the same effective stress as the notched specimen, N_S can be determined from the *S-N* curve, as shown in the Fig. A.1, which is expressed as Eq. (9):

$$\log N_S = -6.01 \cdot \log \sigma_{eff} + 21.45. \quad \cdots\cdots(9)$$

Finally, Eq. (3) combined with Eqs. (5), (7) and (9) can be rewritten as:

$$\frac{N_\mathrm{N}(\sigma_\mathrm{eff})}{N_\mathrm{S}(\sigma_\mathrm{eff})}=(\frac{S_\mathrm{N}\cdot L_\mathrm{CD}}{S_\mathrm{S}\cdot L_\mathrm{FCI}})^{\mu} \quad \cdots\cdots(10)$$

The procedure to calculate the predicted life of notched specimens by the proposed modified HSV method is depicted in Fig. 3.

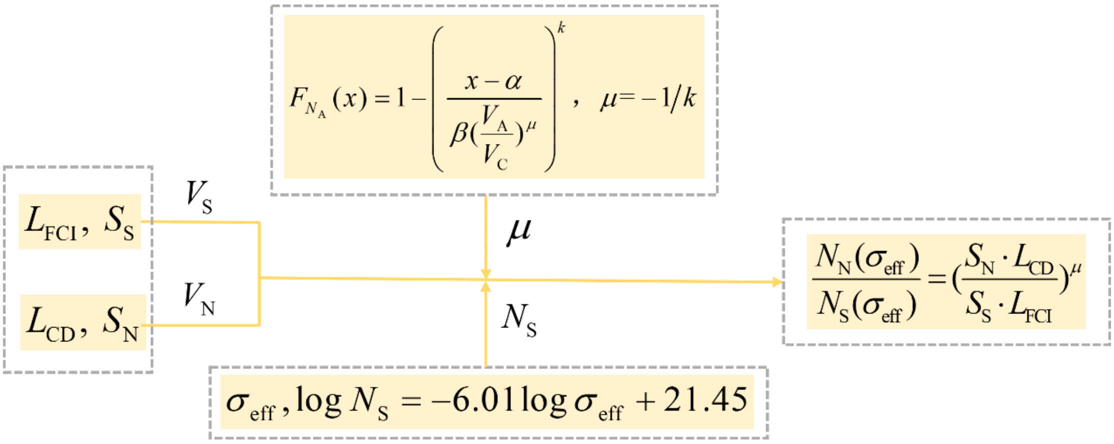

Fig. 3. Procedure to calculate the predicted life of notched specimens by the proposed modified HSV method

3. Experimental validation

3.1 Experimental details

In this study, a widely used industrial steel (quenched and tempered 30CrMnSiA) was used for the experiments. The mechanical properties of this 30CrMnSiA steel are listed in Table1, including Young's modulus *E*, yield strength σ_S, ultimate strength σ_t, and fracture strain ε_f. To predict the fatigue life of the notched specimens, the *S-N* curve of the smooth specimens is plotted. The *S-N* fatigue tests were conducted, at room temperature, according to ASTM E606 [40] under stress control with a stress ratio $R=-1$ and a frequency of 10 Hz. The geometry of the smooth specimens and the fatigue test setup (50 kN MTS) are shown in Fig. 4 (a). The experimental data and *P-S-N* curves are shown in Fig. 4 (b) within

a fatigue life limitation of 5×10^5 cycles, and the scatter bands for three different values of the probability of survival, *Ps* (*i.e.*, *Ps* = 5%, *Ps* = 50% and *Ps* = 95%), are plotted, which are calculated by taking the confidence level equal to 95%. The full separation of the broken specimen was used as failure criterion.

The modified HSV method proposed in Section 2 was verified using the *S-N* fatigue tests of single-notched and multi-notched specimens under the same loading condition as the smooth specimens and the experimental results were compared to the predicted results. The geometries of single-notched and multi-notched specimens and fatigue test setups are shown in Figs. 5 (a) and (b). It is worth nothing that a novel clamp of multi-notched specimens in Fig. 5 (b) was designed to ensure that the load does not become eccentric during clamping. Before the tests, the surfaces of all the specimens were polished in the axial direction down to a roughness of less than 0.2 μm according to ASTM E606 [40]. In addition, in order to identify the fatigue crack initiation region and calculate the critical crack size for the smooth specimens, the fracture surfaces were examined by scanning electron microscopy (SEM) analysis. The critical crack sizes of the notched specimens determined by the fracture surface was compared to that determined by the critical distance.

Table 1. The mechanical properties of 30CrMnSiA steel

Properties	Measure values
E (MPa)	189,855
σ_S (MPa)	960
σ_t (MPa)	1,054
ε_f	16.5%

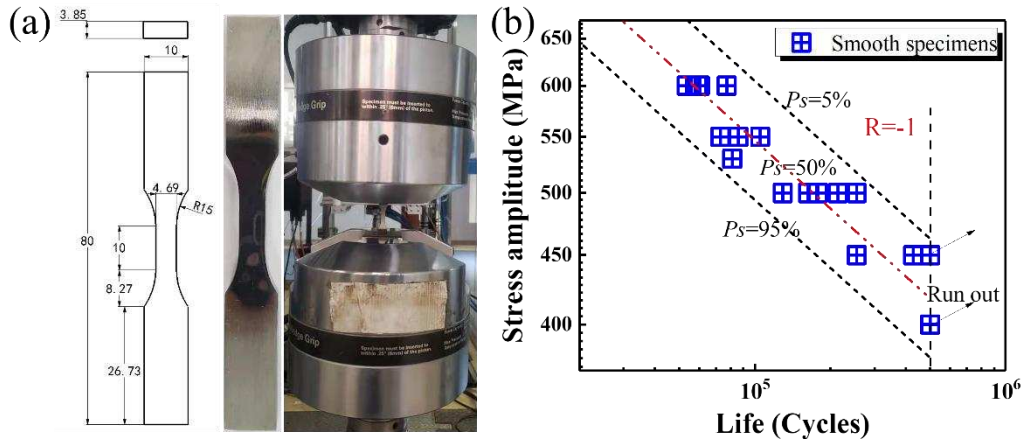

Fig. 4. (a) Smooth specimen dimension, layout and experimental setup; (b) the *S*-*N* curves of smooth specimens to predict the fatigue life of notched specimens.

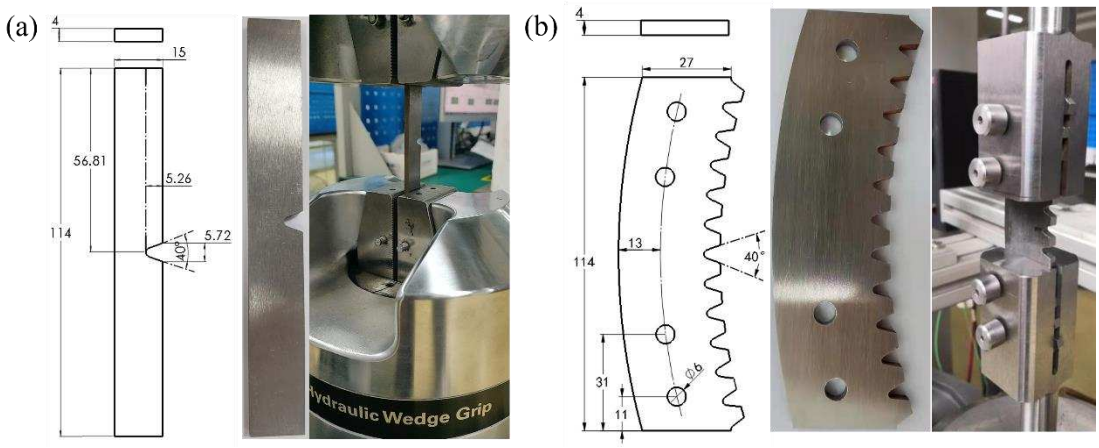

Fig. 5. (a) Single-notched specimen dimension, layout and experimental setup; (b) multi-notched component dimension, layout and experimental setup.

3.2 Parameter determination

3.2.1 Critical crack size determination

To calculate V_N for the final prediction in Eq. (10) for fatigue life, L_{CD} needs to be determined using Eq. (4). ΔK_{th} in Eq. (4) can be obtained by the fatigue crack growth (FCG) test in the threshold region, which was conducted by using the *K*-decreasing method with a stress ratio of $R=-1$ and a frequency of 10 Hz under loading control according to ASTM E647-15e1 [41]. The M(T) specimens (Fig.

6 (a)) were tested using a 100 kN MTS machine at room temperature. As shown in Fig. 6 (b), ΔK_{th} is about 24.6 MPa $\cdot \sqrt{m}$. In addition, using the *S*-*N* curve of smooth specimens in Fig. 4, $\Delta\sigma_0$ was determined to be about 800 MPa. Then, using Eq. (4), the critical distance was calculated to be equal to 0.3 mm. Furthermore, using the fracture surface investigation and V90 criterion, critical crack sizes were also calculated and compared with the critical distance of notched specimens. The fracture surfaces are shown in Figs. 7 (a)-(e), the multiple crack nucleation sites observed suggest that the stress concentration leads to high stress zones at the notch root, which are more prone to plastic slip and dislocation pile up [42-45]. The volume of V90 criterion for multi-notched specimens is shown in Fig. 7 (g), and the stress distribution along the path is shown in Fig. 7 (f). The critical crack sizes obtained by using these two methods are equal to 0.28 and 0.09 mm, respectively, as shown in Fig. 7 (h). Compared with the V90 criterion, the critical distance gives a critical crack size that is closer to that of the experimental fracture surface, indicating that the critical distance is an effective parameter to calculate the HSV.

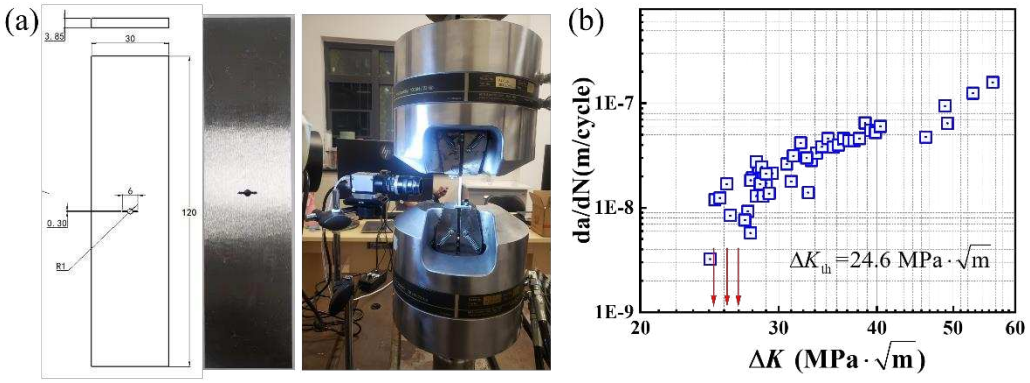

Fig. 6. (a) M(T) specimen dimension, layout and experimental setup; (b) the FCG rate curve in the near-threshold region.

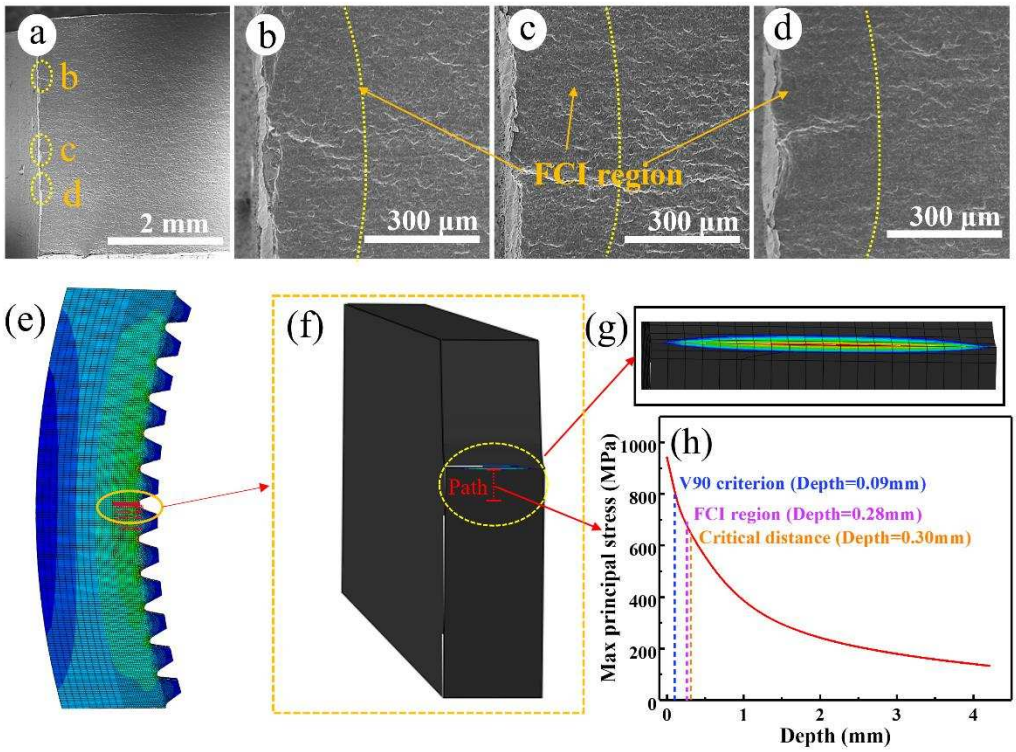

Fig. 7. (a)-(d) The fracture surface of multi-notched specimens with stress amplitude of 100 MPa; (e) the finite element model of multi-notched specimen; (f) the maximum principal stress distribution along the path; (g) the volume of V90 criterion for multi-notched specimens with stress amplitude of 100 MPa, (h) the comparison of critical crack sizes calculated by V90 criterion, FCI region, and critical distance.

To calculate V_S in Eq. (10), L_{FCI} of smooth specimens can be obtained from the fracture surface investigation images shown in Figs. 8 (a), (b), (c), (d). The images reveal that the fracture surface roughness in the crack initiation region is larger than that in crack propagation region due to the development of the persistent slip band. The persistent slip band formation is related to the crack nucleation and short crack propagation, which might account for 90% of the fatigue life. This finding also indicates a different mechanism of crack initiation compared to that of the notched specimen [29].

As shown in Figs. 8 (a)-(d), in the observed single crack nucleation sites the crack initiation sizes along the surface are close under different stress amplitudes, at about 100 μm. In addition, the HSV of smooth specimens using the V90 criterion shown in Fig. 8 (e) occupies essentially the entire gauge section due to its low stress concentration factor [46]. Also, as shown in Fig. 8, compared with the FCI region, the HSV of the smooth specimen will be overestimated by using the V90 criterion leading to a large error in the fatigue life prediction for notched specimens.

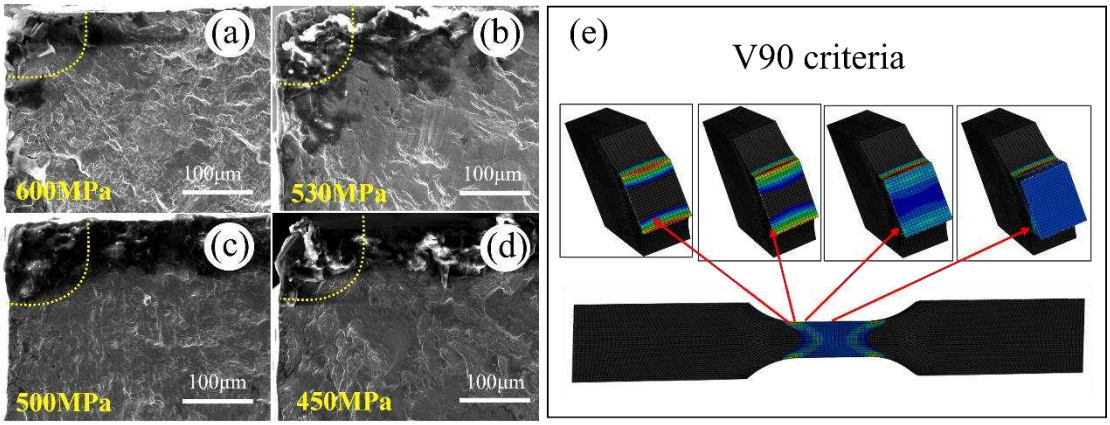

Fig .8. The fracture surface of smooth specimens with the stress amplitudes of (a) 600 MPa, (b) 530 MPa, (c) 500 MPa (d) 450 MPa, and (e) the HSV by using V90 criterion.

3.2.2 Highly stressed surface area determination

ABAQUS software was used to simulate the stress distribution and determine the highly stressed surface areas. A finite element model was built using C3D8R elements, and the stresses applied to the single-notched, multi-notched, and smooth specimens were 135, 80, and 500 MPa, respectively. The results from the simulations are shown in Figs. 9 (a)-(c), respectively. In order to obtain a better representation of the stress gradients that arise in the vicinity of the notch, the size of the elements was reduced to obtain a fine mesh around the center of the notch for single and multi-notched specimens. The stress concentration factors, K_t ($K_t = \sigma_{mp} / \sigma_{appl}$), of the single-notched, multi-notched and smooth specimens were 9.42, 6.57, and 1.1, respectively. Due to the larger K_t of single-notched and multi-

notched specimens, their maximum principal stress caused by a small loading stress are much larger than that of the smooth specimens shown in Fig. 9. In addition, the highly stressed surface areas of single-notched (1.67 mm^2) and multi-notched specimens (11.5 mm^2) are much smaller than that of smooth specimens (239.72 mm^2). As shown in Figs. 9 (a) and (b), for the single-notched specimen, the highly stressed surface area is concentrated around the notch root; but for the multi-notched components, the highly-stressed surface area is concentrated around the middle three tooth roots due to the local stress concentration typically experienced by the notches and their complex stress-strain response. However, for the smooth specimens, the highly stressed surface area is evenly distributed within the gauge section. According to the size effect, the larger highly stressed surface area of smooth specimens has more defects, indicating a lower fatigue life for the smooth specimens than that for the single-notched and multi-notched specimens at the same maximum principal stress.

Moreover, a series of effective stresses σ_{eff} can be obtained according to the stress distribution along the paths shown in Figs. 9 (a) and (b) in the notch vicinities according to Fig. 1. Then, μ in Eq. (10) is determined by fitting the fatigue lives at a same stress amplitude using the Weibull distribution [17], and the fatigue lives can be obtained by transforming the fatigue life under the different stress levels using the *S-N* curve in Fig. 4 with *Ps*=50%.

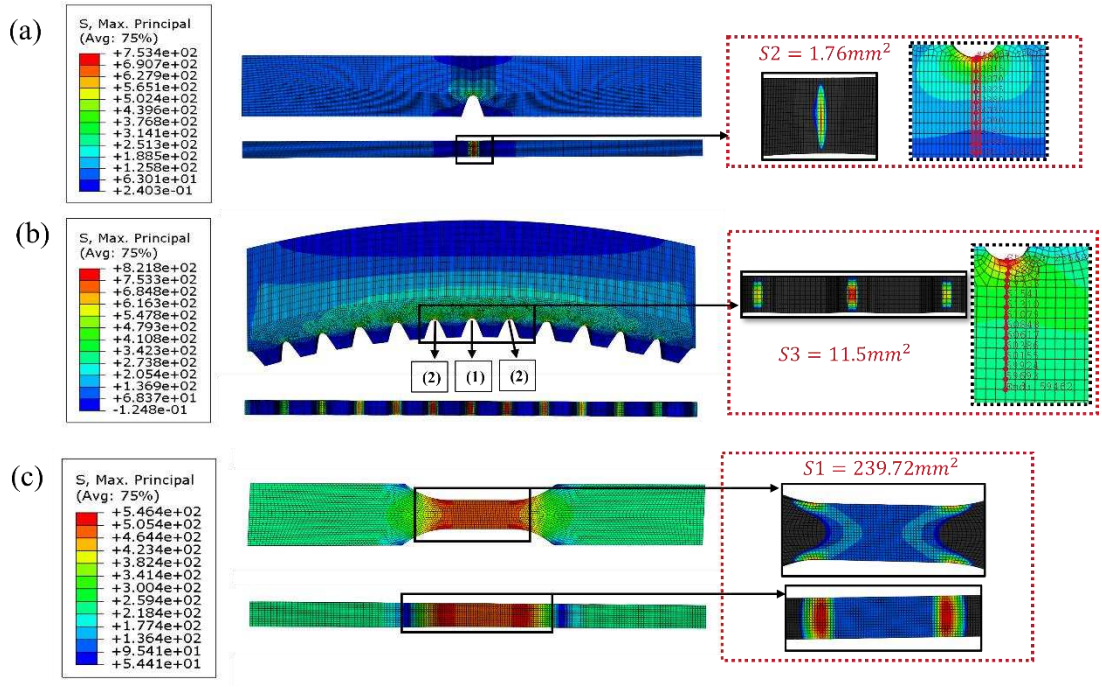

Fig. 9. The distribution of the maximum principal stress of the (a) single-notched specimen; (b) multi-notched specimen; (c) smooth specimen.

3.3 **Model validation**

3.2.3 Model validation for single-notched specimens

The predicted *P-S-N* curves of single-notched specimens are shown in Figs. 10 (a) and (b) obtained by using the traditional HSV method and the modified HSV method, respectively. The experimental data of single-notched specimens is used to validate the proposed modified HSV method. As shown in Fig. 10 (a), the *P-S-N* curves predicted by the traditional HSV method are underestimated as a result of not taking the notch effects into account. The single-notched specimen with high K_t has a steep stress gradient (Fig. 9 (a)), which makes the maximum principal stress much larger than the effective stress. However, compared with the traditional HSV method, most of experimental data obtained by using the modified HSV method lie within the predicted band (Fig. 10 (b)). In addition, the results of the fatigue life predictions by the traditional HSV and modified HSV methods under the *Ps*=50% (listed and

compared in Table 2) reveal that the modified HSV method can more accurately predict the fatigue life of single-notched specimens (with a validity error range from -14.35 to 21.45%), compared with the traditional HSV method (with a validity error range from -37.95 to -12.07%).

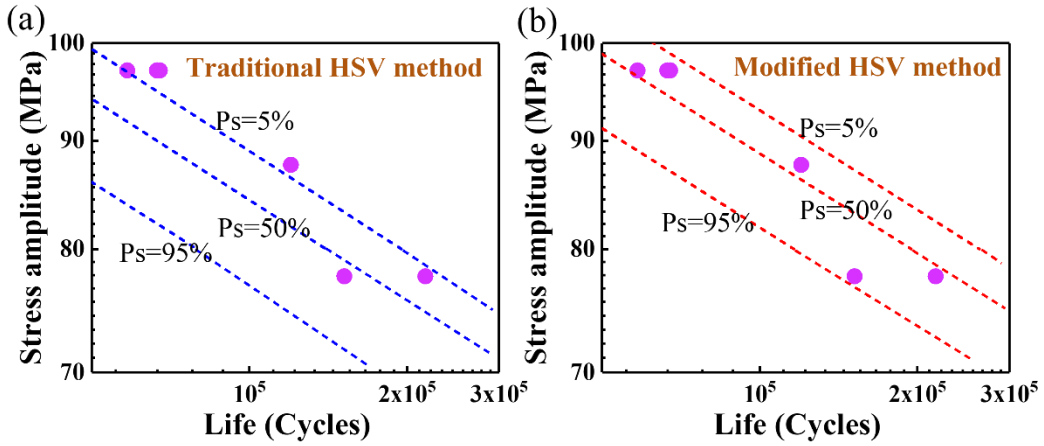

Fig. 10. Predicted *P-S-N* of single-notched specimens: (a) traditional HSV method; (b) modified HSV method.

Table 2. Predicted life lives and their errors of single-notched specimens

Stress amplitude σ (MPa)	Fatigue life (Cycle)			Error (%)	
	Arithmetic average of experimental data	Traditional HSV method (*Ps*=50%)	Modified HSV method (*Ps*=50%)	Traditional HSV method (*Ps*=50%)	Modified HSV method (*Ps*=50%)
97	64160	39810	54954	-37.95	-14.35
88	120042	75857	104712	-36.81	-12.77
78	184337	162181	223872	-12.07	21.45

3.3.2 Model validation for multi-notched specimens

The validation of the proposed modified HSV method for multi-notched configurations was also performed, and the fatigue life predictions of the proposed method was also compared with the conventional methods of HSV and TCD [47]. The TCD method is that modified by Susmel and Taylor [47], in which the critical distance is obtained using the smooth and single-notched calibration *S-N*

fatigue curves shown in Fig. A.1, using Eq. (10) :

$$L = A \cdot N_f^B \text{ ,} \qquad (10)$$

where A, B are the material constants.

The *P-S-N* curves of multi-notched specimens predicted by the traditional HSV method, TCD method and modified HSV method are shown in Figs. 11 (a)-(c), respectively. As shown in Fig. 11 (a), there was an overestimation with the traditional HSV method, which might be attributed to the overestimated HSV of smooth specimens by using V90 criterion. Compared to the single-notch specimen, the low-stress concentration of the multiple notches reduces the notch effect, resulting in an increase in the effect of the HSV. Furthermore, there was also an overestimation by the TCD method, especially in low-cycle fatigue shown in Fig. 11 (b), which can be attributed to the neglect of the size effect. A reported study has shown that more crack nucleation sites occurred at the notch root for high stress level, which will decrease the fatigue life [43]. For the modified HSV method, as shown in Fig. 11 (c), all of the experimental data fall within the predicted *P-S-N* curves, and the scatter index T (T=0.34) calculated using this method is lower than that calculated using the traditional HSV (T=0.36) and TCD (T=0.40) methods. In addition, the *S-N* curves of Ps=50% obtained by using these three methods are shown in Fig. 11 (d) for further comparison purposes. Smaller disagreements with experimental results of the modified HSV method can be observed compared with the other methods, which indicates that the accuracy of the proposed modified HSV model was successfully increased compared with the traditional HSV and TCD methods. Moreover, the bridge for predicting notched specimens from smooth specimens was also well established by considering the critical crack size.

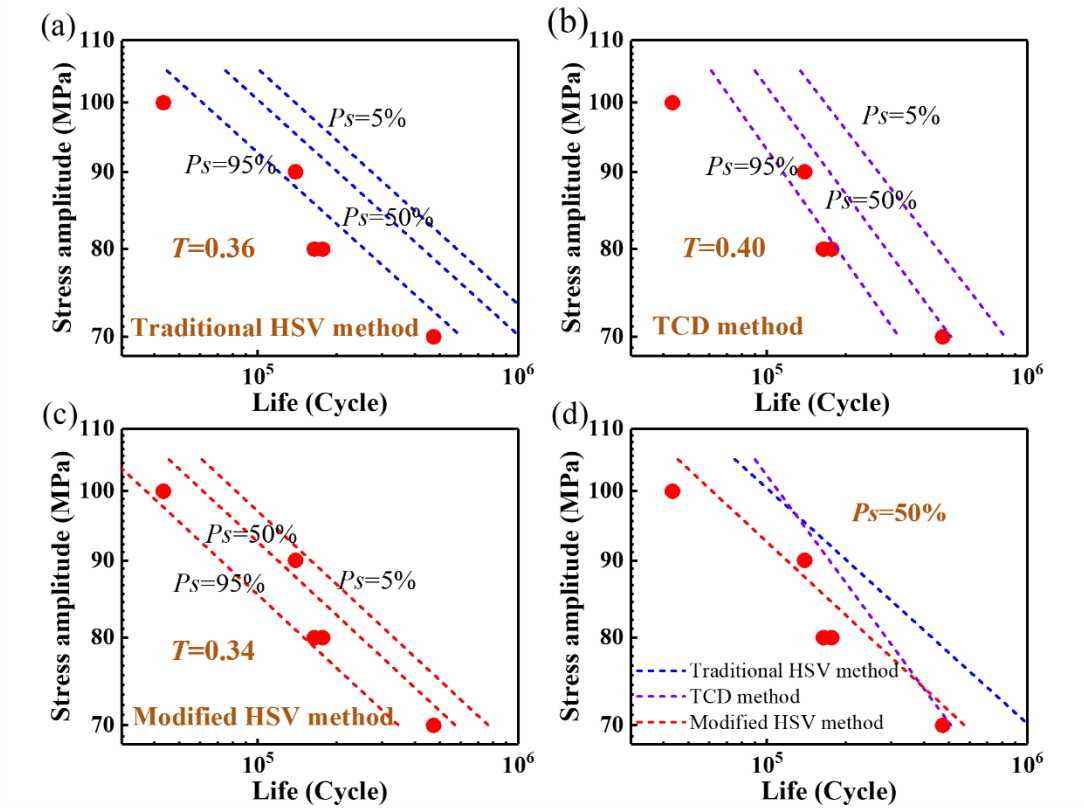

Fig. 11. Predicted *P-S-N* curves of multi-notched specimens by: (a) the traditional HSV method; (b) TCD method; (c) the modified HSV method; (d) tcomparison of *S-N* curves (*Ps*=50%) obtained by the traditional HSV, TCD and modified HSV methods.

4. Conclusions

In this study, a modified HSV method considering the difference between the critical crack sizes of smooth and notched specimens is proposed. Also, the experimental data of the single-notched and multi-notched specimens were used for model validation. The main conclusions are as follows.

(1) A probabilistic HSV model based on the Weibull distribution is developed and used. The highly stressed surface areas are identified, and the Weibull distribution are used to account for the statistical and geometrical size effect.

(2) The critical crack sizes of smooth and notched specimens taking the fatigue initiation regions into

account are proposed. Comparisons with the fracture surfaces and V90 criterion of the smooth and notched specimens shows that the critical crack sizes L_{FCI} and L_{CD} are more accurate to characterize the HSV. In addition, effective stresses estimated by the TCD method are introduced to the HSV method according to the Neuber theory.

(3) The single-notched and multi-notched specimens are used to validate the accuracy and reliability of the modified HSV method. The results show that almost all the experimental data fall within the predicted *P-S-N* curves with 90% survival probability. Smaller scatter index and errors indicate that the accuracy of the prediction model was successfully increased.

Appendix A

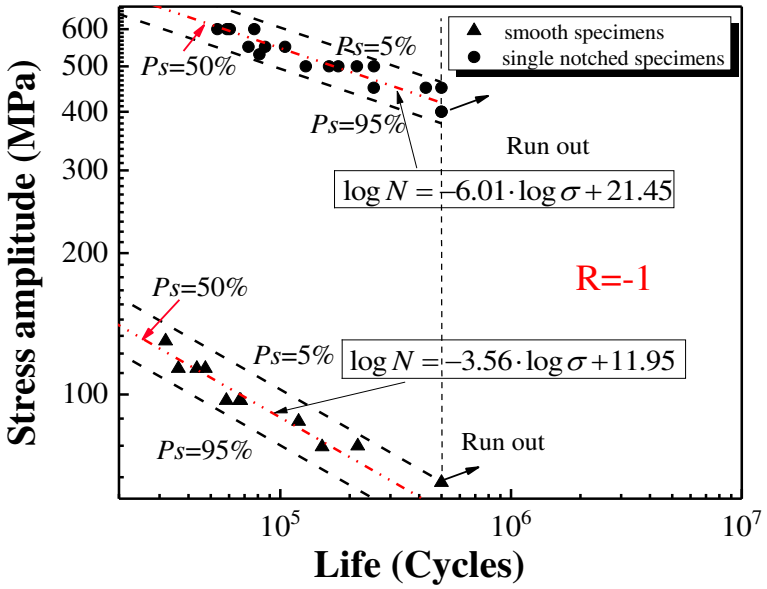

Fig. A.1. The *S-N* curves of smooth and single-notched specimens

5. References

[1] Ramakokovhu U, Desai D, Snedden G. Jamiru T. Significance of residual stresses in fatigue life prediction of micro gas turbine blade. Eng Fail Anal 2021;120.

https://doi.org/10.1016/j.engfailanal.2020.105092.

[2] Hu Z, Berto F, Hong Y, Susmel L. Comparison of TCD and SED methods in fatigue lifetime assessment. Int J Fatigue 2019;123:105–34.

https://doi.org/10.1016/j.ijfatigue.2019.02.009.

[3] Susmel L. The theory of critical distances: a review of its applications in fatigue. Eng Fract Mech 2008;75:1706-1724.

https://doi.org/10.1016/j.engfracmech.2006.12.004.

[4] Yu ZY, Zhu SP, Liu Q, Liu Y. A new energy-critical plane damage parameter for multiaxial fatigue life prediction of turbine blades. Materials 2017;10(5):513.

https://doi.org/10.3390/ma10050513.

[5] Sih GC. Strain energy density factor applied to mixed-mode crack problems. Int J Fract 1974;10:305–21.

https://doi.org/10.1007/BF00035493.

[6] Taylor D, Bologna P, Bel Knani K. Prediction of fatigue failure location on a component using a critical distance method. Int J Fatigue 2000;22(9):735–42

https://doi.org/10.1016/S0142-1123(00)00062-1.

[7] Van Hooreweder B, Moens D, Boonen R, Sas P. Fatigue strength analysis of notched aluminium specimens using the highly stressed volume method. Fatigue Fract Eng Mater Struct 2011;35(2):154–9

https://doi.org/10.1111/j.1460-2695.2011.01602.x.

[8] Sonsino CM, Kaufmann H, Grubisic V. Transferability of material data for the example of a randomly loaded forged truck stub axle. SAE Trans 1997;106(5):649–70

https://doi.org/10.4271/970708.

[9] Waterkotte R, Baumgartner J, Sonsino CM. Fatigue assessment of laserbeam welded PM steel components by the notch stress approach. Materialwiss Werkstofftech 2011;42(10):881–7. https://doi.org/10.1002/mawe.201100861.

[10] Ai Y, Zhu SP, Liao D, Correia JAFO, De Jesus AMP, Keshtegar B. Probabilistic modelling of notch fatigue and size effect of components using highly stressed volume approach. Int J Fatigue 2019;127:110–119. https://doi.org/10.1016/j.ijfatigue.2019.06.002.

[11] Kuguel R. The highly stressed volume of material as a fundamental parameter in the fatigue strength of metal members. Theor Appl Fract Mech 1960;169:1–18.

[12] Lin CK, Lee WJ. Effects of highly stressed volume on fatigue strength of austempered ductile irons. Int J Fatigue 1998;20:301–307. https://doi.org/10.1016/S0142-1123(97)00134-5.

[13] Grell WA, Niggeler GH, Groskreutz ME, Laz PJ. Evaluation of creep damage accumulation models: considerations of stepped testing and highly stressed volume. Fatigue Fract Eng Mater Struct 2007;30:689–97. https://doi.org/10.1111/j.1460-2695.2007.01135.x

[14] Khoukhi DEL, Morel F, Saintier N, Bellett D, Osmond P. The effect of microstructural heterogeneities on the high cycle fatigue scatter of cast aluminium alloys: from an elementary volume to the structure. MATEC web of conferences 2018. https://doi.org/10.1051/matecconf/201816514006.

[15] He JC, Zhu SP, Taddesse AT, Niu X. Evaluation of critical distance, highly stressed volume, and weakest-link methods in notch fatigue analysis. Int J Fatigue 2022;162.

https://doi.org/10.1016/j.ijfatigue.2022.106950.

[16] Hertel O, Vormwald M. Statistical and geometrical size effects in notched members based on weakest-link and short-crack modelling. Eng Fract Mech 2012;95:72-83.

https://doi.org/10.1016/j.engfracmech.2011.10.017.

[17] Sun C, Zhang X, Liu X, Hong Y. Effects of specimen size on fatigue life of metallic materials in high-cycle and very-high-cycle fatigue regimes. Fatigue Fract Eng Mater Struct 2016;39:770-779.

https://doi.org/10.1111/ffe.12415.

[18] Gui X, Gao G, An B, Misra R.D.K, Bai B. Relationship between non-inclusion induced crack initiation and microstructure on fatigue behavior of bainite/martensite steel in high cycle fatigue/very high cycle (HCF/VHCF) regime. Mater. Sci. Eng. A 2021;803.

https://doi.org/10.1016/j.msea.2020.140692.

[19] Lukas P, Kunz L. Small cracks – nucleation, growth and implication to fatigue life. Int J Fatigue 2003;25(9–11):855–62.

https://doi.org/10.1016/S0142-1123(03)00133-6.

[20] Cui W. A state-of-the-art review on fatigue life prediction methods for metal structures. Int. J. Mech. Sci. 2002;7(1):43–56.

https://doi.org/10.1007/s007730200012.

[21] Shang DG, Xing WY, Jun WD A new approach to the determination of fatigue crack initiation size. Int J Fatigue 1998;20(9):683–687.

https://doi.org/10.1016/S0142-1123(98)00035-8.

[22] Stadnick S, Morrow J. Techniques for smooth specimen simulation of the fatigue behavior of notched members, in: Testing for prediction of material performance in structures and components.

ASTM International 1972.

https://doi.org/10.1520/STP34686S.

[23] Meng L, Yang M, Chen X, Hu Y, Feng M. Physically short fatigue crack growth from notch described by plasticity-corrected stress intensity factor. Int. J. Mech. Sci. 2020;176.

https://doi.org/10.1016/j.ijmecsci.2020.105544.

[24] Neuber H. Theory of notch stresses: principles for exact calculation of strength with reference to structural form and material. USAEC Office of Technical Information 1958.

[25] Taylor D. Analysis of fatigue failures in components using the theory of critical distances. Eng Fail Anal 2005;12:906-914.

https://doi.org/10.1016/j.engfailanal.2004.12.007.

[26] Razavi SMJ, Ferro P, Berto F, et al. Fatigue strength of blunt V-notched specimens produced by selective laser melting of Ti-6Al-4V. Theor Appl Fract Mech 2018;97:376–84.

https://doi.org/10.1016/j.tafmec.2017.06.021

[27] Qian G, Lei WS, Niffenegger M, González-Albuixech VF. On the temperature independence of statistical model parameters for cleavage fracture in ferritic steels. Philos Mag 2018;98:959-1004.

https://doi.org/10.1080/14786435.2018.1425011.

[28] Kang G, Luo H, Review on fatigue life prediction models of welded joint. Acta Mech Sin 2020; 36: 701-726.

https://doi.org/10.1007/s10409-020-00957-0.

[29] Wang Y, Meletis EI, Huang H. Quantitative study of surface roughness evolution during low-cycle fatigue of 316L stainless steel using Scanning Whitelight Interferometric (SWLI) Microscopy. Int J Fatigue 2013;48:280-288.

https://doi.org/10.1016/j.ijfatigue.2012.11.009.

[30] Shyam A, Milligan WW. Effects of deformation behavior on fatigue fracture surface morphology in a nickel-base superalloy. Acta Mater. 2004;52:1503-1513.

https://doi.org/10.1016/j.actamat.2003.11.032.

[31] Macek W, Marciniak Z, Branco R, Rozumek D, Krolczyk ´ GM. A fractographic study exploring the fracture surface topography of S355J2 steel after pseudo-random bending-torsion fatigue tests. Measurement 2021;178:109443.

https://doi.org/10.1016/j.measurement.2021.109443.

[32] Bomas H, Linkewitz T, Mayr P. Application of a weakest-link concept to the fatigue limit of the bearing steel SAE 52100 in a bainitic condition. Fatigue Fract Eng Mater Struct 1999;22:733-741.

https://doi.org/10.1046/j.1460-2695.1999.t01-1-00211.x.

[33] Przybilla C, Fernández-Canteli A, Castillo E. An iterative method to obtain the specimen-independent three-parameter Weibull distribution of strength from bending tests. Procedia Eng 2011;10:1414–1419.

https://doi.org/10.1016/j.proeng.2011.04.235.

[34] Lamela MJ, Fernández Canteli A, Przybilla C, Menendez M. Contrast of a probabilistic design model for laminated glass plates. Mater Sci Forum 2012; 730–732: 501–6.

https://doi.org/10.4028/www.scientific.net/MSF.730-732.501.

[35] Blason S, Muniz-Calvente M, Koller R, Przybilla C, Fernández-Canteli A. Probabilistic assessment of fatigue data from shape homologous but different scale specimens. Application to an experimental program. Eng Fract Mech 2017;185:193–209.

https://doi.org/10.1016/j.engfracmech.2017.05.017.

[36] Xin H, Veljkovic M. Fatigue crack initiation prediction using phantom nodes-based extended finite element method for S355 and S690 steel grades. Eng Fract Mech 2019;214:164-176. https://doi.org/10.1016/j.engfracmech.2019.04.026.

[37] He JC, Zhu SP, Liao D, Niu XP, Gao JW, H.-Z. Huang HZ. Combined TCD and HSV approach for probabilistic assessment of notch fatigue considering size effect. Eng Fail Anal 2021;120. https://doi.org/10.1016/j.engfailanal.2020.105093.

[38] Macek W. Fracture surface formation of notched 2017A-T4 aluminium alloy under bending fatigue. Int J Fract 2021;234:141-157. https://doi.org/10.1007/s10704-021-00579-y.

[39] Susmel L, Taylor D. A novel formulation of the theory of critical distances to estimate lifetime of notched components in the medium-cycle fatigue regime. Fatigue Fract Eng Mater Struct 2007;30:567-581. https://doi.org/10.1111/j.1460-2695.2007.01122.x.

[40] ASTM, ASTM E606: standard practice for strain-controlled fatigue testing. ASTM international, West Conshohocken, PA 2012.

[41] ASTM E647-15e1, Standard test method for measurement of fatigue crack growth rates. ASTM International 2015. https://doi.org/10.1520/E0647-00.

[42] Wang R, Li D, Hu D, Meng F, Liu H, Ma Q. A combined critical distance and highly-stressed-volume model to evaluate the statistical size effect of the stress concentrator on low cycle fatigue of TA19 plate. Int J Fatigue 2017;95:8-17. https://doi.org/10.1016/j.ijfatigue.2016.10.003.

[43] Htoo AT, Miyashita Y, Otsuka Y, Mutoh Y, Sakurai S. Variation of local stress ratio and its effect on notch fatigue behavior of 2024-T4 aluminum alloy. Int J Fatigue 2016;88:19-28. https://doi.org/10.1016/j.ijfatigue.2016.03.001.

[44] Sangid MD. The physics of fatigue crack initiation. Int J Fatigue 2013;57:58-72. https://doi.org/10.1016/j.ijfatigue.2012.10.009.

[45] Qian G, Hong Y, Zhou C. Investigation of high cycle and Very-High-Cycle Fatigue behaviors for a structural steel with smooth and notched specimens. Eng Fail Anal 2010;17:1517-1525. https://doi.org/10.1016/j.engfailanal.2010.06.002.

[46] Leitner M, Vormwald M, Remes H. Statistical size effect on multiaxial fatigue strength of notched steel components. Int J Fatigue 2017;104:322-333. https://doi.org/10.1016/j.ijfatigue.2017.08.002.

[47] Susmel L, Taylor D. The theory of critical distances to predict static strength of notched brittle components subjected to mixed-mode loading. Eng Fract Mech 2008; 75:534-550. https://doi.org/10.1016/j.engfracmech.2007.03.035.